# Analysis and Implementation of an HPF Electronic Ballast for HID Lamps With LFSW Voltage

Hung-Liang Cheng, *Member, IEEE*, Chin-Sien Moo, *Member, IEEE*, Chung-Sheng Yang, and Chun-Kai Huang

***Abstract*—In this paper, a novel high power-factor electronic ballast for metal-halide (MH) lamps based on integration of a buck-boost converter, a buck converter, and a full-bridge inverter is proposed. The buck-boost converter that serves as a power-factor corrector (PFC) is designed to operate at discontinuous conduction mode to achieve a high power factor at the input line. A bidirectional buck converter formed by a full-bridge inverter, an inductor, and a capacitor drives an MH lamp with a low-frequency square-wave voltage to prevent the lamp from acoustic resonance. The lamp power is controlled by adjusting the duty ratio of the active switches of the PFC. The circuit operation is analyzed in detail to derive the design equations. Circuit parameters are designed based on design considerations in practical applications. Finally, a prototype electronic ballast for a 70-W MH lamp is built and tested. Satisfactory performances are obtained from the experimental results.**

***Index Terms*—Acoustic resonance, electronic ballast, low-frequency square-wave (LFSW), metal-halide (MH) lamp, power factor.**

## I. Introduction

Among various kinds of high-intensity discharge (HID) lamps, metal-halide (MH) lamps have the advantages of long lamp life, high luminous efficacy, good color rendition, and have been widely used in many lighting applications [1]–[5]. Since MH lamps have the characteristics of negative incremental impedance, ballasts are required to stabilize the lamp current. With the rapid development of power electronics, high-frequency electronic ballasts have numerously replaced the traditional electromagnetic ones to reduce the size and weight and improve the efficacy of the ballast circuit and light performance in recent years [6]–[12].

However, MH lamps driven by a high-frequency electronic ballast may suffer from problematic acoustic resonance that may lead to arc instability, light fluctuation, or extinguishment, and even cracking the arc tube [8]–[12]. Many approaches have been proposed to solve the problem of acoustic resonance. Among them, driving MH lamps with a low-frequency square-wave (LFSW) voltage has been considered the most effective method to eliminate the occurrence of acoustic resonance for its high reliability and control simplicity [13]–[16]. On the other hand, in order to comply with the more stringent regulations on current harmonics, such as IEC61000-3-2 standards, and to improve the power factor, an ac/dc converter that performs as a power-factor corrector (PFC) is required in ballast circuits. A boost converter or a buck-boost converter is preferred to serve as a PFC. Since the output dc voltage of the PFC is usually higher than the operating voltage of an MH lamp, an additional buck converter should be cascaded after the PFC to comply with the lamp voltage. For these reasons, many proposed electronic ballasts consist of three stages, which are the PFC, the buck converter, and the full-bridge inverter [8], [17], [18].

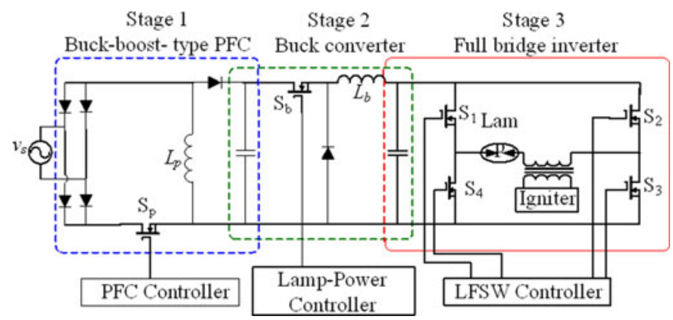


Fig. 1. Three-stage electronic ballast.

Fig. 1 is one example of a three-stage electronic ballast. A buck-boost PFC is followed by a buck converter that regulates the dc-link voltage for the full-bridge inverter and thereby controls the lamp power. The active switches in both the first and the second stages are operated at a high frequency to reduce the size of the magnetic components, while those of the full-bridge inverter are operated at a low frequency to drive the MH lamp with an LFSW current. Although such three-stage electronic ballasts can achieve a high power factor (HPF) and avoid acoustic resonance, they are not cost-effective products. Much of the literature has successfully integrated the buck converter and the full-bridge inverter into one-stage as two-stage electronic ballasts [19]–[22]. These two-stage electronic ballasts consist of a PFC stage and an integrated stage. In spite of their good performance, the two-stage approaches require two individual control circuits and components for both stages. Much of the literature had presented single-stage electronic ballasts by integrating a

Manuscript received August 29, 2011; revised November 15, 2011 and January 13, 2012; accepted February 7, 2012. Date of current version June 20, 2012. This work was supported by the National Science Council (NSC) of Taiwan, Taiwan, under Grant NSC 99-2221-E-214 -074 -MY2. Recommended for publication by Associate Editor S. Y. Hui.

H.-L. Cheng is with the Department of Electrical Engineering, I-Shou University, Kaohsiung 84001, Taiwan (e-mail: hlcheng@isu.edu.tw).

C.-S. Moo is with the Power Electronics Laboratory, Department of Electrical Engineering, National Sun Yat-sen University, Kaohsiung 80424, Taiwan (e-mail: mooxx@mail.ee.nsysu.edu.tw).

C.-S. Yang is with the Department of Telecom Power Module R&D, Acbel Polytech Inc., Tamsui, Taipei, Taiwan (e-mail: Ph3632@gmail.com).

C.-K. Huang is with the R&D Center, Longsun Technologies Co., Ltd, Tainan, Taiwan (e-mail: ken310@mail.longsun.tw).

Color versions of one or more of the figures in this paper are available online at http://ieeexplore.ieee.org.

Digital Object Identifier 10.1109/TPEL.2012.2188545

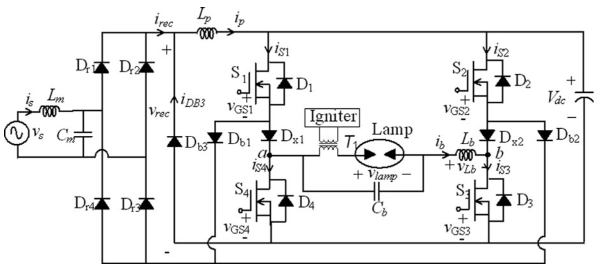


Fig. 2. Proposed HPA electronic ballast.

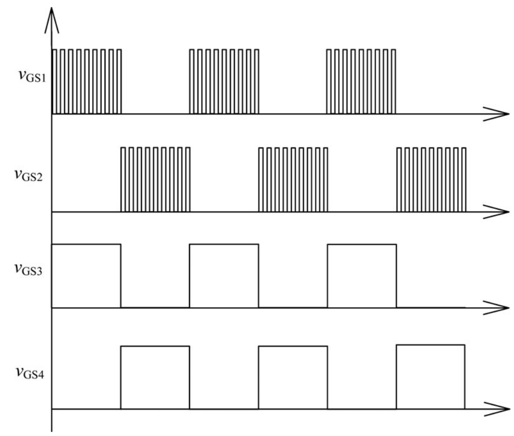

Fig. 3. Time sequence of gated voltages.

PFC and an inverter [23]–[25]. Their outputs are high-frequency sinusoidal voltages, not LFSW ones. They cannot avoid the possibility of appearance of acoustic resonance when driving MH lamps. The literature works [16] and [26] successfully integrated all the three stages and proposed single-stage solutions, where a boost converter or a buck converter is adopted as the PFC stage. Operating a boost converter at a constant frequency and discontinuous conduction mode (DCM) can obtain a unity power factor, provided that its dc-link voltage is much higher than the amplitude of the ac input voltage. High dc-link voltage would result in more switching loss and requires using semiconductors of high voltage rating. Contrarily, if a buck convert is served as a PFC, an HPF can be achieved on condition that its dc output voltage is much smaller than the amplitude of the ac input voltage. Hence, a transformer is required to build up the dc voltage for the inverter stage.

In order to further reduce the component count and hence lower the product cost, this paper proposes an electronic ballast that is derived by integrating a buck-boost-type PFC, a buck converter, and a full-bridge inverter into a single power conversion circuit. Only four active switches are required in the proposed configuration. The buck converter and the full-bridge inverter form a bidirectional buck converter to drive an MH lamp with an LFSW voltage. The lamp is operated at the rated power by regulating the duty ratio of the high-frequency switches. A prototype circuit designed for driving a 70-W MH lamp was built and tested to verify the analytical predictions. Satisfactory performance is obtained from the experimental results.

## II. Circuit Configuration and Operation

In the three-stage electronic ballast circuit, as shown in Fig. 1, each stage has its own active switch(es) with an associated control circuit. The component count can be effectively reduced if the active switches in different stages are shared. Fig. 2 shows the proposed electronic ballast that is derived by integrating the active switches in Fig. 1. Four MOSFETs, namely, $S_1$, $S_2$, $S_3$, and $S_4$ with intrinsic body diodes, $D_1$, $D_2$, $D_3$, and $D_4$, serve as the active switches of the full-bridge inverter, which are controlled by four gated signals, namely, $v_{GS1}$, $v_{GS2}$, $v_{GS3}$, and $v_{GS4}$, respectively.

Fig. 3 illustrates the time sequence of the control logic. The bottom switches are gated by $v_{GS3}$ and $v_{GS4}$ at a low frequency with a short dead time. The upper switches are gated by $v_{GS1}$ and $v_{GS2}$. It is seen that $v_{GS1}$ and $v_{GS2}$ are high-frequency rectangular-wave voltages when $v_{GS3}$ and $v_{GS4}$ are at high voltage level, respectively. The dead time prevents the upper switches and the bottom ones from conducting current simultaneously. The control circuit is shown in Fig. 4. The LM324 consists of four independent operational amplifiers. Two of them are use to detect the zero-crossing point of the input ac voltage and then, generate a low-frequency square voltage that is synchronous with the ac input. A high-frequency square voltage is generated from the TL494 that is a fixed frequency, pulsewidth modulation (PWM) controller. The L6384 receives the low-frequency voltage from LM324 and generates two complementary low-frequency square voltages between which there is a short dead time controlled by connecting a resistor between pin 3 and ground. The low-frequency and the high-frequency square voltages are "AND" by the 7408. Four devices TLP250 form the full-bridge gate driver circuit for the MOSFETs $S_1$–$S_4$ in Fig. 2.

In Fig. 4, the low-frequency square voltages, $v_{GS3}$ and $v_{GS4}$, are synchronized with the line frequency (60 Hz). Thus, the lamp operation is also synchronized with the line frequency. Since the input voltage is rectified and then fed to the next stage for power processing, the operation of $S_3$ and $S_4$ does not need to synchronize with the line frequency. Their frequency could be raised for operating the lamp at a higher frequency to improve light quality. It is noted that there should be a short dead time between $v_{GS3}$ and $v_{GS4}$. During the dead time, all switches are OFF and no current is drawn from the input line. It hampers the input current to be sinusoidal. Increasing the frequency of $v_{GS3}$ and $v_{GS4}$ would increase the deviation of the input current from a sinusoidal waveform and then reduce the effect of power-factor correction.

The input power and lamp power are controlled by regulating the duty ratio of the upper switches, $S_1$ and $S_2$. This duty ratio, namely $D_1$, is proportional to the pulsewidth of $v_{GS1}$ and $v_{GS2}$. Fig. 4 shows that the lamp power is open loop controlled. $D_1$ is adjusted by the variable resistor connected to Pin 4 of TL494. Actually, Pin 4 controls the dead time of the output pulse of TL494. The longer the dead time is, the smaller the duty ratio is. For achieving a constant lamp power, a closed-loop control must be used when the input voltage fluctuates. If a closed-loop control is supposed to used, the variable resistor connected to

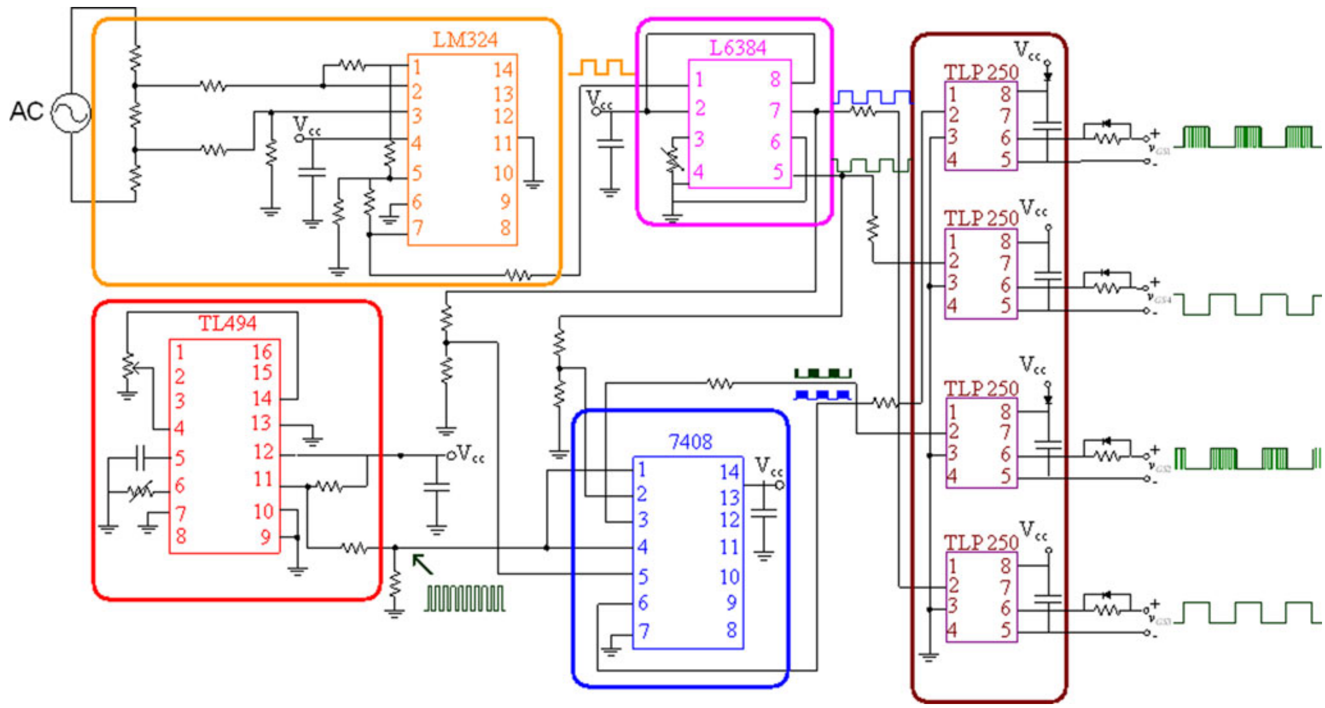


Fig. 4. Control circuit.

Pin 4 should be removed. Then, a closed-loop control for output PWM could be accomplished by monitoring and feeding the dc-link voltage $V_{\rm dc}$ to the error amplifier in TL494. Generally, the three-stage electronic ballast allows the soft start of the entire system. The proposed electronic ballast can meet this purpose by setting a longer dead time of the output pulse of TL494 at startup, and then slowly reducing the dead time to increase the duty ratio of $S_1$ and $S_2$. By so doing, the input power can be slowly increased at startup to achieve the soft start.

Power factor correction is performed by the buck-boost converter formed by $S_1$ and $S_2$, and three additional diodes, $D_{b1}$, $D_{b2}$, and $D_{b3}$, with an inductor $L_p$ and the dc-link capacitor $C_1$. By operating the buck-boost PFC at DCM at a fixed switching frequency, a unity power factor at the input line can be achieved. The lamp power is regulated by a bidirectional buck converter formed by $C_1$, the four active switches ($S_1$–$S_4$) and two diodes $D_{x1}$ and $D_{x2}$ with an output filter formed by an inductor $L_b$ and a capacitors $C_b$. Since $S_1$ and $S_2$ are switched ON and OFF at a high frequency, the components $L_p$, $L_b$, and $C_b$ can be small. It helps to reduce the product size and weight. An LFSW voltage across $C_b$ can be obtained by operating $S_3$ and $S_4$ at a low frequency. The high-frequency components of the inverter output voltage $v_{ab}$ can be filtered out by $C_b$ and $L_b$. An igniter with the transformer $T_1$ generates a high voltage to start up the lamp. A small low-pass filter ($L_m$ and $C_m$) is used to remove the high-frequency current harmonics at the input line.

For simplifying the circuit analysis, the low-pass filter, the igniter circuit, and transformer $T_1$ are omitted, and the MH lamp is represented by its equivalent resistance $R_{\rm lamp}$. In addition, following assumptions are made:

1) all the circuit components are ideal;
2) the capacitance of $C_1$ is large enough so that the dc-link voltage $V_{\rm dc}$ can be regarded as a voltage source;
3) the capacitance $C_b$ is large enough so that the voltage across it remains almost constant in a high-frequency switching cycle;
4) the lamp is regarded as an open circuit before ignition, and a pure resistance at the steady-state operation.

Both the buck-boost converter and the bidirectional buck converter are designed to operate at DCM. The circuit operation can be divided into two categories depending on the states of $S_3$ and $S_4$. The corresponding operation modes are shown in Fig. 5(a) and (b), respectively. At the steady state, the circuit operation can be divided into four modes in a high-frequency cycle. Since the operations in Fig. 5(a) and (b) are similar to each other, only the operation modes in Fig. 5(a) are discussed. Fig. 6 illustrates the theoretical waveforms for each mode. The circuit operation is described as follows.

### A. Mode I ($t_0 < t < t_1$)

This mode begins at the instant of turning ON the active switch $S_1$. The rectified input voltage $v_{\rm rec}$ is imposed on the inductor $L_p$. Since the buck-boost converter is designed to operate at DCM, the inductor current $i_p$ increases linearly from zero with a rising slope that is proportional to $v_{\rm rec}$. $S_3$ operates at a low frequency and keeps at the ON state. The voltage across the inductor $L_b$ is equal to ($V_{\rm dc} - v_{\rm lamp}$). The buck converter is also operated at DCM, and thus, $i_b$ rises from zero linearly. The capacitor $C_1$ supplies a current through $S_1$, $D_{x1}$, and $S_3$ to charge $C_b$.

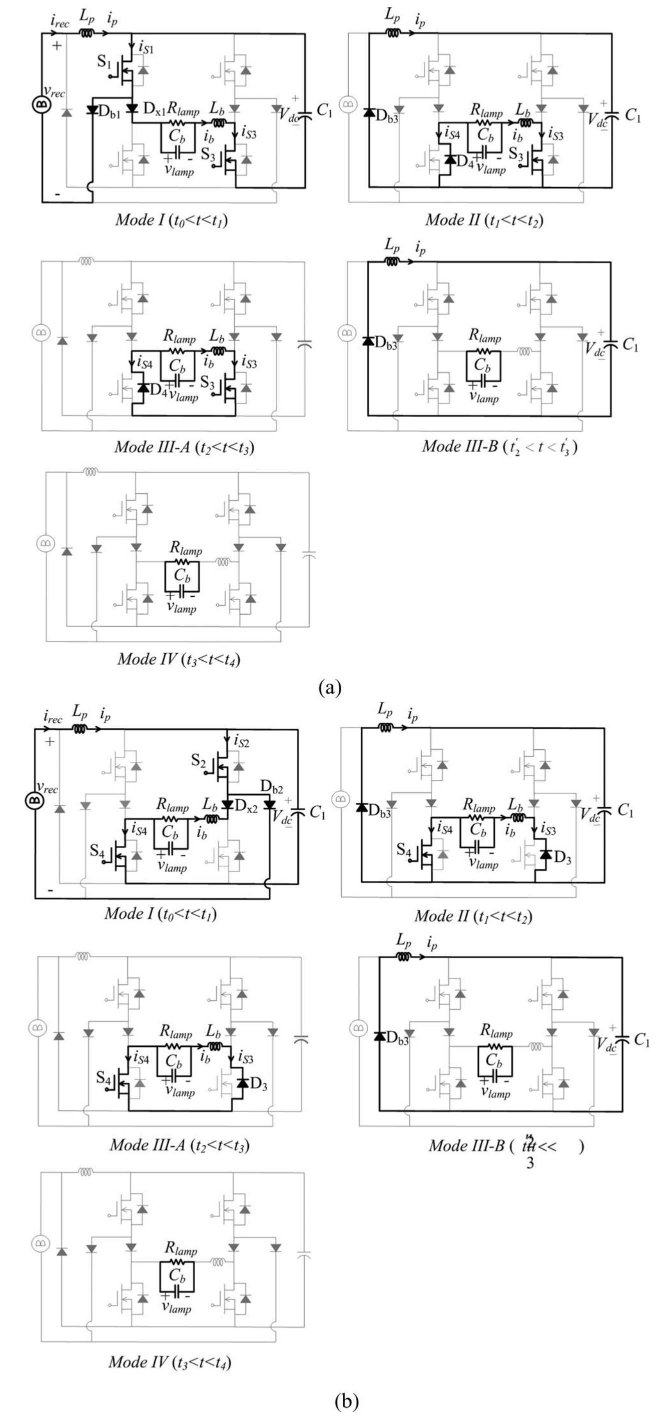


Fig. 5. Operation modes. (a) $S_3$ is ON. (b) $S_4$ is ON.

### B. *Mode II* ($t_1 < t < t_2$)

The circuit operation enters this mode at the instant of turning OFF $S_1$. $S_3$ remains at ON state. $i_p$ will freewheel through diode $D_{b3}$ to charge $C_1$. Meanwhile, $i_b$ flows through $S_3$ and $D_4$ to supply current to $C_b$ and the lamp. The voltages across $L_p$ and $L_b$ are equal to $-V_{\mathrm{dc}}$ and $-v_{\mathrm{lamp}}$, respectively. Therefore, both currents decrease linearly.

As stated in Mode II, the rising slope of $i_p$ is proportional to $v_{\mathrm{rec}}$. The higher $v_{\mathrm{rec}}$ is, the higher the peak value of $i_p$ is.

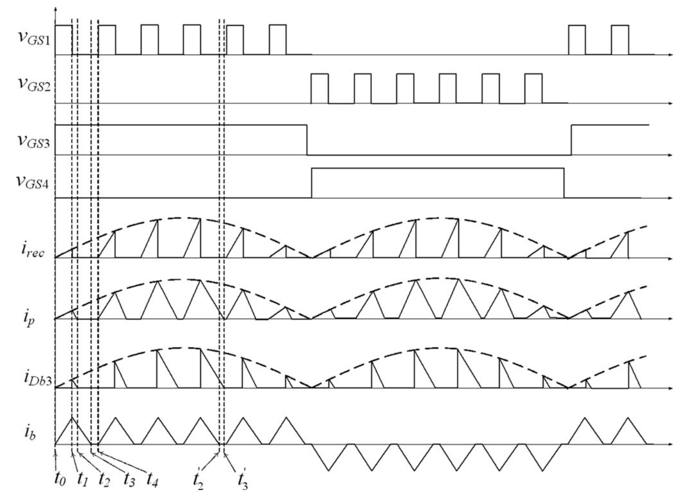


Fig. 6. Theoretical waveforms.

Therefore, the time duration for $i_p$ declining to zero is not a constant but varies with $v_{\mathrm{rec}}$. On the contrary, the rising and the declining slopes of $i_b$ are both constant. The time duration for $i_b$ to decline to zero is also constant. Thus, there could be two possible modes following *Mode II*, depending on which current, $i_p$ or $i_b$, reaches zero first.

### C. *Mode III-A* ($t_2 < t < t_3$)

When $v_{\mathrm{rec}}$ is at a low level, the peak value of $i_p$ is low. Under this condition, $i_p$ will decline to zero before $i_b$ does. As soon as $i_p$ reaches zero, the circuit operation enters *Mode III-A*. During this mode, only $i_b$ and the lamp current keep flowing and $i_b$ decreases continuously. When $i_b$ reaches zero, *Mode III-A* ends and the circuit operation enters *Mode IV*.

### D. *Mode III-B* ($t_2' < t < t_3'$)

On the contrary, when $v_{\mathrm{rec}}$ is at a high level, the peak of $i_p$ is also high. It will take a longer time for $i_p$ to decline to zero. Therefore, $i_p$ may decline to zero later than $i_b$ does. The circuit operation will enter *Mode III-B* when $i_b$ reaches zero. In this mode, $i_p$ keeps flowing through $D_{b3}$ to charge $C_1$ while $C_b$ supplies current for the lamp. This mode ends at the time when $i_p$ reaches zero and the circuit operation enters *Mode IV*.

### E. *Mode IV* ($t_3 < t < t_4$)

During this mode, both $i_p$ and $i_b$ are zero. Only the lamp current is supplied from $C_b$. When $S_1$ is turned ON again, the circuit operation returns to *Mode I* of the next high-frequency cycle.

Based on the circuit operation, the proposed electronic ballast can reduce the energy-processing steps as compared with the three-stage one. It helps to reduce the circuit loss. However, two active switches are saved at the expense of increasing the number of diodes from 2 to 5. Also, $S_1$ and $S_2$ have higher current stress since they should share the current paths in the buck-boost, buck, and output inverter. Adding diodes in the current paths and high current will result in more conduction loss.

## III. Circuit Analysis

Based on the circuit operation described in Section II, the currents flowing in the buck-boost converter and the bidirectional buck converter do not interfere with each other even though some active switches are shared. The features of the buck-boost converter and the buck converter can be retained. Therefore, the buck-boost PFC and the buck converter can be analyzed separately.

### A. Buck-Boost Power-Factor Corrector

The PFC is supplied from an ac line-voltage source

$$v_s(t) = V_m \sin(2\pi f_L t) \tag{1}$$

where $f_L$ and $V_m$ are the frequency and amplitude of the line-voltage source, respectively. In practice, $f_L$ is much lower than the high switching frequency, $f_s$, of $S_1$ and $S_2$. It is reasonable to consider the rectified input voltage as a constant over a high-frequency cycle. During *Mode I*, either $S_1$ or $S_2$ is turned ON. Since the buck-boost convert is operated at DCM over an entire line-frequency cycle, $i_p$ increases linearly from zero and can be expressed as

$$i_p(t) = \frac{V_{\rm rec}(t)}{L_p} t = \frac{V_m\,|\sin(2\pi f_L t)|}{L_p} t,\ \ 0 \le t \le D_1 T_s \tag{2}$$

where $T_s$ is the high-frequency switching period and $D_1$ is the duty ratio of $S_1$ and $S_2$. At the end of *Mode I*, $i_p$ reaches a peak value

$$i_{p,\rm peak}(t) = \frac{V_m\,|\sin(2\pi f_L t)|\, D_1 T_s}{L_p}. \tag{3}$$

The waveform of the rectified current $i_{\rm rec}$ and $i_p$ are conceptually shown in Fig. 7. Current $i_{\rm rec}$ is equal to $i_p$ during *Mode I*, and keeps zero in other modes. It means that $i_{\rm rec}$ is equal to the rising part of $i_p$. The high-frequency contents of $i_{\rm rec}$ are removed by the low-pass filter. Then, the input current $i_s$ is equal to the average of $i_{\rm rec}$ over a high-frequency cycle

$$i_s(t) = \frac{1}{T_s}\int_0^{T_s} i_{\rm rec}(t)\cdot d(t) = \frac{V_m T_s D_1^2}{2L_p}\sin(2\pi f_L t). \tag{4}$$

As comparing (1) and (4), it is noticed that the input current is a sinusoidal waveform and in phase with the input-line voltage if the duty ratio remains constant over an entire line cycle. As a result, an HPF is achieved. The input power can be obtained by taking average of its instantaneous value over one line-frequency cycle

$$P_{\rm in} = \frac{1}{2\pi}\int_0^{2\pi} v_s(t)\cdot i_s(t)\, d(2\pi f_L t) = \frac{V_m^2 D_1^2}{4 L_p f_s}. \tag{5}$$

Then, the lamp power can be calculated as

$$P_{\rm lamp} = \eta \cdot P_{\rm in} = \frac{\eta V_m^2 D_1^2}{4 L_p f_s} \tag{6}$$

where $\eta$ represents the circuit conversion efficiency.

To operate the buck-boost converter at DCM, the following inequality equation should be met:

$$V_m\,|\sin(2\pi f_L t)|\cdot D_1 T_s - V_{\rm dc}(1-D_1)T_s \le 0. \tag{7}$$

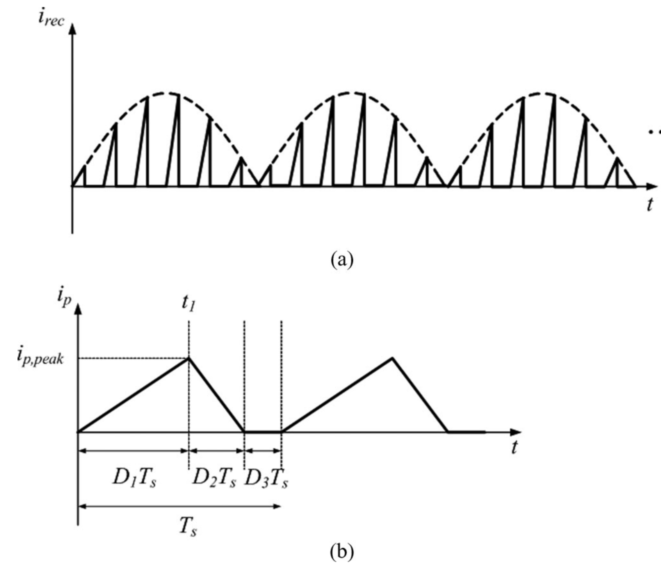


Fig. 7. Theoretical waveforms of (a) $i_{\rm rec}$, and (b) $i_p$ in high-frequency cycles.

From (7), $V_{\rm dc}$ should be designed to be high enough to ensure DCM operation over an entire input line-frequency cycle

$$V_{\rm dc} \ge V_m \cdot \frac{D_1}{1-D_1}. \tag{8}$$

### B. Bidirectional Buck Converter

According to the discussion on the circuit operation in Section II, $S_1$–$S_4$, $D_{x1}$, $D_{x2}$, $L_b$ and $C_b$ form a bidirectional buck converter. The inductor $L_b$ and capacitor $C_b$ can filter out the high-frequency components of the inverter output voltage $v_{ab}$. Then, the voltage across $C_b$ is a low-frequency square waveform. Fig. 8 shows the equivalent circuits of the bidirectional buck converter. In Fig. 8(a), $S_2$ and $S_4$ are OFF. $S_3$ is kept ON and $S_1$ is turned ON and OFF at a high frequency. In Fig. 8(b), $S_1$ and $S_3$ are OFF. $S_4$ is kept ON and $S_2$ is turned ON and OFF at a high frequency. Since the operations in Fig. 8(a) and (b) are similar except that the polarities of $i_b$ and $v_{\rm lamp}$ are reversed, only the circuit operation in Fig. 8(a) is discussed.

When $S_1$ and $S_3$ are ON, the voltage across inductor $L_b$ is

$$v_{Lb} = V_{\rm dc} - v_{\rm lamp}. \tag{9}$$

The inductor current $i_b$ rises from zero and will reach a peak value at the instant of turning OFF $S_1$. Its peak value is

$$i_{b,\rm peak} = \frac{(V_{\rm dc} - V_{\rm lamp})\, D_1 T_S}{L_b}. \tag{10}$$

When $S_1$ is turned OFF, $i_b$ freewheels through diode $D_4$. The voltage across $L_b$ is

$$v_{Lb} = -V_{\rm lamp}. \tag{11}$$

This negative voltage causes $i_b$ to decrease. The duration for $i_b$ decreasing from the peak value to zero is

$$T_{\rm off} = \frac{(V_{\rm dc} - V_{\rm lamp})\, D_1 T_S}{V_{\rm lamp}}. \tag{12}$$

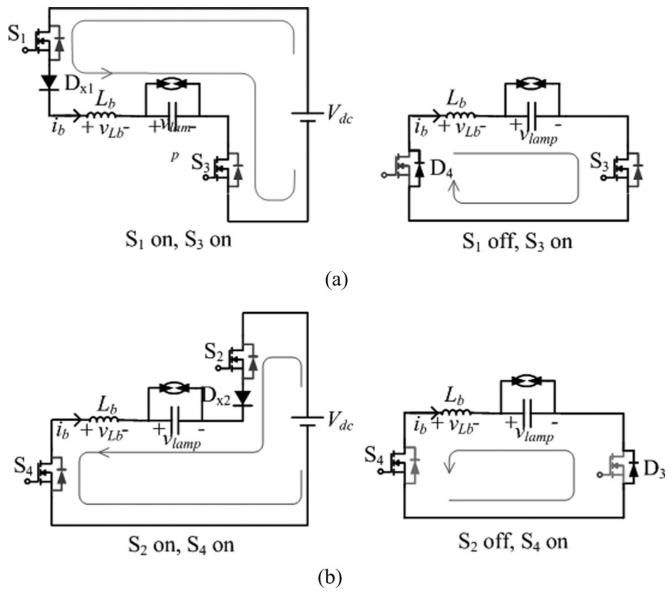


Fig. 8. Equivalent circuit of buck converter. (a) $S_3$ is ON. (b) $S_4$ is ON.

TABLE I
CIRCUIT SPECIFICATIONS

| | |
|---|---|
| $v_s$ | 110 ±10% $V_{rms}$, 60 Hz |
| $f_{S1}, f_{S2}$ | 30 kHz |
| $f_{S3}, f_{S4}$ | 60 Hz |
| $P_{lamp}$ | 70-W |
| $V_{lamp}$ | 85 V |
| $I_{lamp}$ | 0.82 A |
| $R_{lamp}$ | 103.6 Ω |

For DCM operation, $T_{\rm off}$ should be shorter than $(1-D_1)T_s$. It means that $V_{\rm dc}$ cannot be too high and should be designed to meet the following equation:

$$V_{\rm dc} \le \frac{V_{\rm lamp}}{D_1}. \tag{13}$$

As can be seen in Fig. 6, $i_b$ is a triangular waveform. The average value in a high-frequency cycle can be expressed as

$$\overline{i_b} = \frac{(V_{\rm dc} - V_{\rm lamp})V_{\rm dc} D_1^2 T_S}{2L_b V_{\rm lamp}}. \tag{14}$$

At the steady state, the average value of $i_b$ is equal to lamp current

$$\overline{i_b} = \frac{V_{\rm lamp}}{R_{\rm lamp}}. \tag{15}$$

Combining (14) and (15), $L_b$ can be obtained as

$$L_b = \frac{(V_{\rm dc} - V_{\rm lamp})V_{\rm dc} D_1^2 T_S R_{\rm lamp}}{2V_{\rm lamp}^2}. \tag{16}$$

## IV. PARAMETERS DESIGN

An electronic ballast for a 70-W MH lamp is illustrated as a design example. Table I lists the circuit specifications. The input voltage is 110 ± 10 % $V_{\rm rms}$. The switching frequency of $S_1$ and $S_2$ is 30 kHz while that of $S_3$ and $S_4$ is 60 Hz. The lamp voltage and current at the rated power are 85 V and 0.82 A, respectively. The design considerations are outlined as follows.

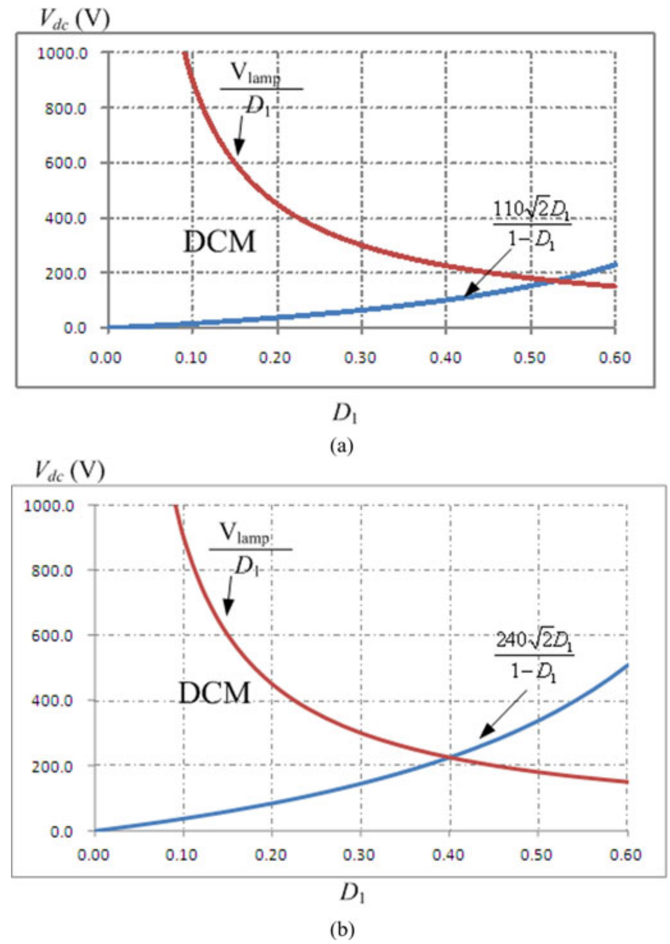


Fig. 9. Relation curves of $V_{\rm dc}$ versus $D_1$ for DCM operation at (a) $v_s$ = 110 $V_{\rm rms}$, $V_{\rm lamp}$ = 85 V and (b) $v_s$ = 240 $V_{\rm rms}$, $V_{\rm lamp}$ = 85 V.

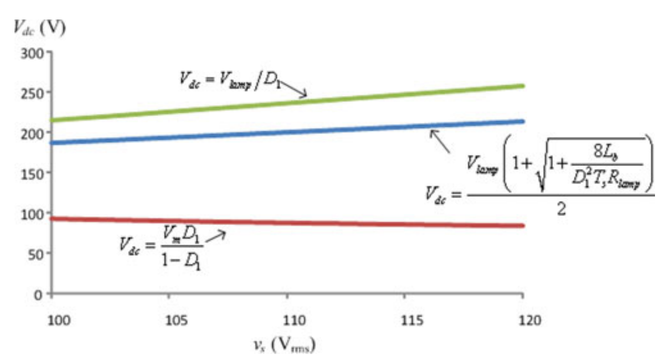


Fig. 10. Relation curves of $V_{\rm dc}$ versus $v_s$.

*1) Step 1 (Choose $V_{\rm dc}$ and $D_1$):* Equations (8) and (13) show the boundary conditions for operating the buck-boost converter and the buck converter at DCM, respectively. Fig. 9(a) is an illustrative example with $v_s$ = 110 $V_{\rm rms}$ and $V_{\rm lamp}$ = 85 V. Between these curves, DCM operation is ensured for both converters. From (6), the lamp power can be regulated by adjusting

TABLE II
VOLTAGE/CURRENT STRESS IN THE DIFFERENT SEMICONDUCTORS

| | Voltage stress | | Current Stress | |
|---|---|---|---|---|
| | Theoretical Formula | Calculated Value | Theoretical Formula | Calculated Value |
| $D_{r1}, D_{r2}, D_{r3}, D_{r4}$ | $V_m$ | 155 V | $V_m D_1 T_s / L_p$ | 6 A |
| $D_{b1}, D_{b2}$ | $V_{dc}$ | 200 V | $V_m D_1 T_s / L_p$ | 6 A |
| $D_{b3}$ | $V_m + V_{dc}$ | 355 V | $V_m D_1 T_s / L_p$ | 6 A |
| $D_{x1}, D_{x2}$ | $V_m$ | 155 V | $(V_{dc} - V_{lamp}) D_1 T_s / L_b$ | 1.9 A |
| $S_1, S_2$ | $V_m + V_{dc}$ | 355 V | $V_m D_1 T_s / L_p + (V_{dc} - V_{lamp}) D_1 T_s / L_b$ | 7.9 A |
| $S_3, S_4$ | $V_{dc}$ | 200V | $(V_{dc} - V_{lamp}) D_1 T_s / L_b$ | 1.9 A |

$D_1$. In this case, $D_1$ should be less than 0.52. Besides, $V_{\rm dc}$ should be designed as low as possible to reduce voltage stress and switching loss on circuit components. In this illustrative design example, $V_{\rm dc}$ and $D_1$ are chosen to be

$$V_{\rm dc} = 200\,{\rm V}, \quad D_1 = 0.36.$$

It is noted that this proposed electronic ballast is suitable for higher line voltages (220–240 $V_{\rm rms}$). Fig. 9(b) shows the boundary curves for DCM operation of both converters with $v_s = 240$ $V_{\rm rms}$ and $V_{\rm lamp} = 85$ V. As compared with Fig. 9(a), the applicable range of $D_1$ in Fig. 9(b) is reduced at a high input voltage. Although the designed values, $V_{\rm dc} = 200$ V and $D_1 = 0.36$, can still meet the DCM requirement, a higher $V_{\rm dc}$ and a smaller $D_1$ are preferred for the consideration of design margin.

*2) Step 2 (Calculate $L_p$ and $L_b$):* Using (6) and (16) and assuming 85% circuit efficiency, $L_p$ and $L_b$ are calculated to be

$$L_p = 0.31\,{\rm mH}, \quad L_b = 0.71\,{\rm mH}.$$

*3) Step 3 (Calculate $V_{\rm dc}$ for 110 ± 10 % $V_{\rm rms}$ input voltage):* Equation (16) can be rewritten as

$$V_{\rm dc} = \frac{V_{\rm lamp}\left(1 + \sqrt{1 + (8L_b / D_1^2 T_S R_{\rm lamp})}\right)}{2}. \tag{17}$$

From (6), $D_1$ is inversely proportional to the input voltage for achieving constant lamp power. It means that $D_1$ should change from 0.4 to 0.33 when $v_s$ changes from 100 to 120 $V_{\rm rms}$.

Using (6), (13), and (17), the relation curve of $V_{\rm dc}$ versus $v_s$ can be obtained and plotted in Fig. 10, showing that DCM operation is maintained for the input voltage ranged from 100 to 120 $V_{\rm rms}$.

*4) Step 4 (Calculate $C_b$):* To prevent acoustic resonance occurring, the energy caused by the lamp current ripple should be small. It requires $C_b$ be large enough to reduce the voltage ripple, and hence, reduce the current ripple. The voltage ripple of the lamp voltage is expressed as [27]

$$\frac{\Delta V_{\rm lamp}}{V_{\rm lamp}} = \frac{(1-D)T_S^2}{8L_b C_b} \times 100\%. \tag{18}$$

In order to have a voltage ripple lower than 15%, $C_b$ is calculated to be larger than 0.83 $\mu$F. A large $C_b$ would result in low voltage ripple. However, the voltage across $C_b$ changes polarity in every low-frequency cycle. In the transient time for $C_b$ to change the polarity, high-value $C_b$ would induce higher transient current

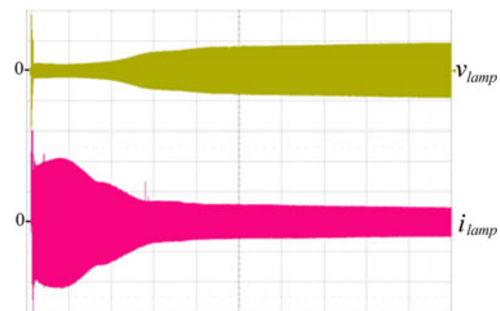


Fig. 11. Lamp voltage and current during starting transient ($v_{\rm lamp}$: 100 V/div, $i_{\rm lamp}$: 2 A/div, time: 10 s/div).

and longer transient time for charging $C_b$ to a stable value. There should be a compromise between having low voltage ripple and low transient current. Here, $C_b$ is chosen to be

$$C_b = 1.0\,(\mu{\rm F}).$$

## V. EXPERIMENTAL RESULTS

A prototype of the proposed electronic ballast was built and tested with the circuit parameters as follows:

$$L_m = 2\,{\rm mH}, \; C_m = 0.5\,\mu{\rm H}, \; L_p = 0.31\,{\rm mH}, \; L_b = 0.71\,{\rm mH}$$

$$C_b = 1.0\,\mu{\rm F}, \quad C_{\rm dc} = 330\,\mu{\rm F}, \quad S_1 -- S_4 : {\rm 2SK2843}$$

$$D_{b1}, D_{b2}, D_{b3}, D_{x1}, D_{x2} : {\rm MUR460}.$$

Table II shows the theoretical formulas and calculated values of the voltage and current stresses in the different semiconductors when the proposed electronic ballast operates at the stead-steady state. Here, the transient spikes of the current and voltage are ignored.

Fig. 11 shows the lamp voltage and current during the starting transient. After igniting the lamp, it takes about 50 s to initiates the thermal equilibrium and finally reaches the steady-state operation at the rated lamp power. Fig. 12 shows the waveforms of the input voltage and current at 110 $V_{\rm rms}$ input voltage. The input current is sinusoidal and in phase with the input voltage. The circuit efficiency is 87%. The power factor is higher than 0.99 and the total current harmonic distortion (THD) is less than 5%. Fig. 13 shows the currents in the buck-boost converters and the buck converter. It is seen that these converters can all operate at DCM over an entire cycle of the line source. Nevertheless,

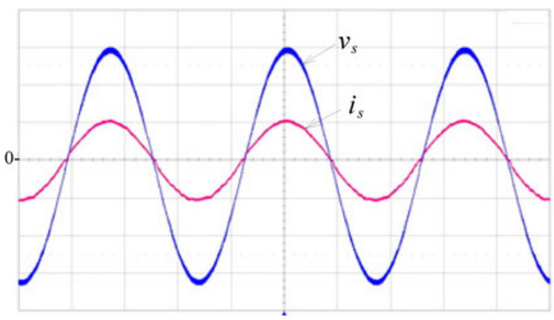


Fig. 12. Input line voltage and current ($v_s$: 50 V/div, $i_s$: 1 A/div, time: 5 ms/div).

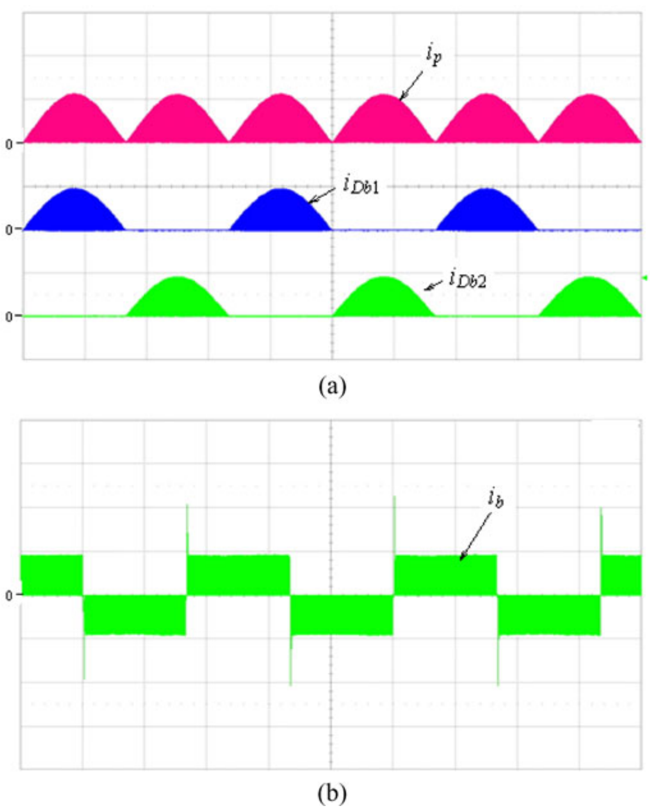


Fig. 13. (a) Currents in the buck-boost converters ($i_p$ : 5 A /div, $i_{Db1}$ : 5 A/div, $i_{Db2}$ : 5 A/div, time: 5 ms/div). (b) current in the buck converter ($i_b$: 2 A/div, time: 5 ms/div).

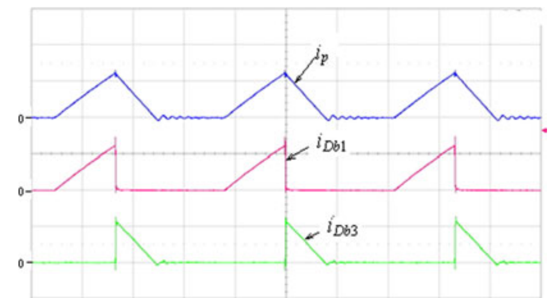


Fig. 14. Currents of the buck-boost converter in high-frequency cycles ($i_p$: 5 A /div, $i_{Db1}$: 5 A/div, $i_{Db3}$: 5 A/div, time: 10 $\mu$s/div).

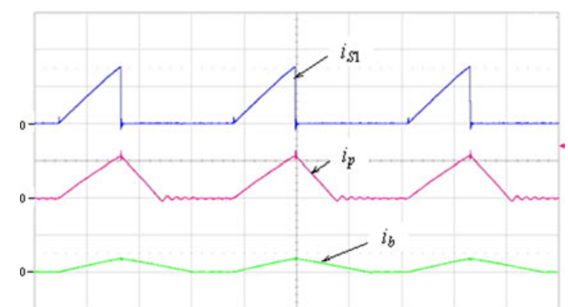


Fig. 15. Waveforms of $i_{S1}$, $i_p$, and $i_b$ ($i_{S1}$: 5 A /div, $i_p$: 5 A/div, $i_b$: 5 A/div, time: 10 $\mu$s/div).

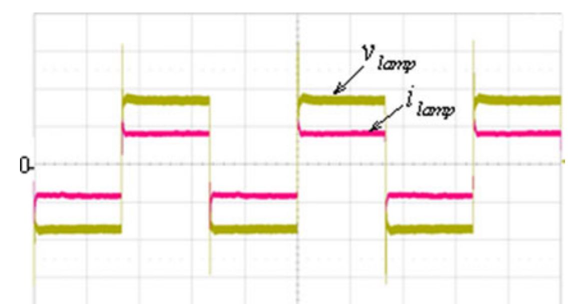


Fig. 16. Lamp voltage and current ($v_{\mathrm{lamp}}$: 50 V/div, $i_{\mathrm{lamp}}$: 1 A/div, time: 5 ms/div).

the buck-boost converter and the buck converter have high peak current at DCM operation. The measured peak currents are 6.0 and 1.9 A, respectively. Fig. 14 shows the currents of the buck-boost converter in some high frequency. It verifies the operation of the buck-boost converter. Fig 15 shows the current flowing through active switch $S_1$ and the inductor currents of the buck-boost and the buck converters. Since the active switch is shared by these converters, $i_{S1}$ is equal to the sum of $i_p$ and $i_b$ when $S_1$ is ON. The waveforms of lamp voltage and current shown in Fig. 16 indicate that the lamp is driven by a 60-Hz square current. The high-frequency waveforms of lamp voltage and current are shown in Fig. 17. The measured values of the voltage and current ripples are 10.5%. The lamp power ripple related to the lamp rated power is calculated to be 10.5%. The lamp is operated stably and free from acoustic resonance. Much of the literature claims that acoustic resonance can be triggered by much smaller periodical input power if lamps are aged. From (18), using a larger $C_b$ can reduce the voltage ripple. However, a large $C_b$ would induce higher transient current. The voltage and current waveforms of the upper and the bottom switches are shown in Fig. 18. When $S_1$ is turned OFF, the voltage across $S_1$ is $V_{\mathrm{dc}}$ plus the voltage across $C_b$. When $S_3$ is turned OFF, the voltage across $S_3$ is equal to $V_{\mathrm{dc}}$. It is observed that when the inductor currents of the converters decline to zero, these voltages oscillate owing to the effect of parasitic capacitance and inductance.

## VI. Conclusion

A novel high power-factor electronic ballast for driving MH lamps with an LFSW voltage is presented. The proposed

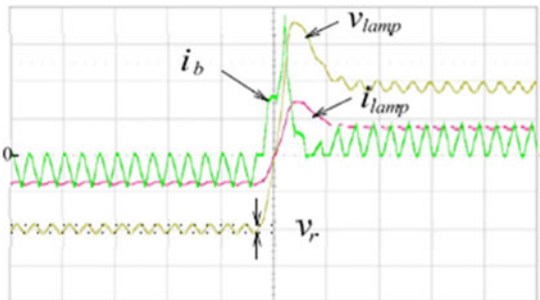


Fig. 17. $v_{\rm lamp}$, $i_{\rm lamp}$, and $i_b$ during low-frequency transient ($v_{\rm lamp}$: 50 V/div, $i_{\rm lamp}$: 1 A/div, $i_b$: 2 A/div, time: 100 us/div).

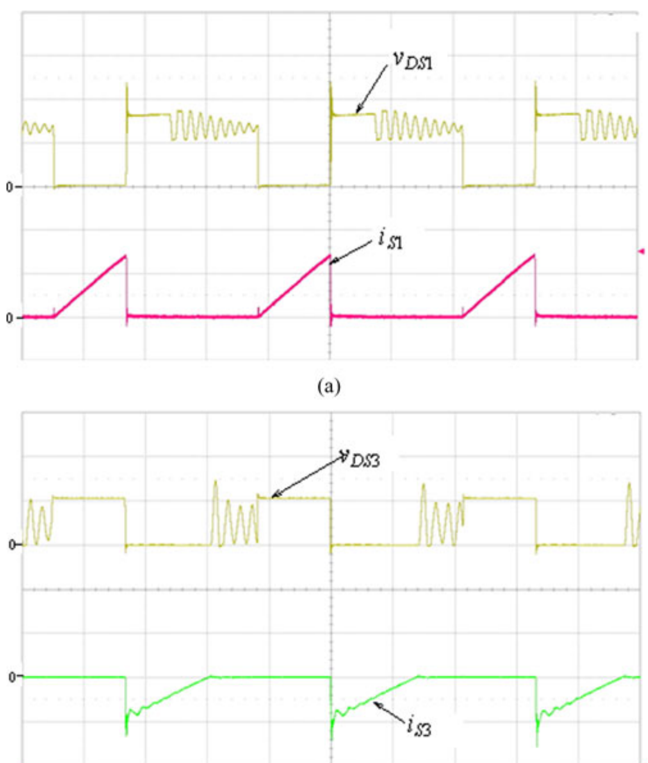


(a)

(b)

Fig. 18. Voltage and current waveforms of (a) upper switch ($v_{DS1}$: 200 V/div, $i_{S1}$: 5 A/div, time: 10 $\mu$s/div) and (b) bottom switch ($v_{DS3}$: 200 V /div, $i_{S3}$: 2 A/div, time: 10 $\mu$s/div).

circuit is derived by integrating a buck-boost converter, a buck converter, and a full-bridge inverter into a single stage. The buck-boost converter performs as a PFC and operates at DCM to achieve an HPF and low THD. The circuit operations are described and the design equations are derived. A prototype circuit designed for a 70-W MH lamp was built and measured to verify the theoretical analyses. Experimental results show that the electronic ballast performs satisfactorily. A nearly unity power factor and low THD can be achieved. The lamp is driven by an LFSW current to avoid the occurrence of acoustic resonance.

## References

[1] C. M. Huang, T. J. Liang, R. L. Lin, and J. F. Chen, "A novel constantpower control circuit for HID electronic ballast," *IEEE Trans. Power Electron.*, vol. 22, no. 3, pp. 854–862, May 2007.

[2] K. F. Kwok, K. W. Eric Cheng, and D. Ping, "Generalstudy for design the HID ballasts," in *Proc. IEEE Int. Conf. Power Electron. Syst. Appl.*, Nov., 2006, pp. 182–185.

[3] A. N. Bhoj and M. J. Kushner, "Plasma dynamics during breakdown in an HID lamp," *IEEE Trans. Plasma Sci.*, vol. 33, no. 2, pp. 518–519, Apr. 2005.

[4] K. C. Paul, T. Takemura, T. Hiramoto, A. Erraki, F. Dawson, G. Zissis, J. J. Gonzalez, A. Gleizes, M. S. Benilov, and J. D. Lavers, "Self-consistent model of HID lamp for design applications," *IEEE Trans. Plasma Sci.*, vol. 34, no. 4, pp. 1536–1547, Aug. 2006.

[5] C. S. Moo, S. Y. Tang, W. T. Tsai, and H. L. Cheng, "Acceleration scenarios of metal halide lamps," *IEEE Trans. Plasma Sci.*, vol. 36, no. 4, pp. 1907–1912, Aug. 2008.

[6] M. A. Dalla Costa, J. M. Alonso, J. García, J. Cardesín, and M. Rico-Secades, "Acoustic resonance characterization of low-wattage metal-halide lamps under low-frequency square-waveform operation," *IEEE Trans. Power Electron.*, vol. 22, no. 3, pp. 735–743, May 2007.

[7] Y. T. Huang, S. T. Chen, C. R. Lee, H. J. Li, and L. L. Lee, "Designs and implementation of the dimmable electronic ballast for metal-halide lamps," in *Proc. IEEE Ind. Electron. Soc.*, Nov. 2007, pp. 1352–1356.

[8] T. J. Liang and C. M. Huang, "Interleaving controlled three-leg electronic ballast for dual-HID-lamps," *IEEE Trans. Power Electron.*, vol. 23, no. 3, pp. 1401–1409, May 2008.

[9] M. Ponce, A. Lopez, J. Correa, J. Arau, and J. M. Alonso, "Electronic ballast for HID lamps with high frequency square waveform to avoid acoustic resonances," in *Proc. IEEE Appl. Power Electron. Conf. Expo.*, 2001, vol. 2, pp. 658–663.

[10] J. C. Á. Antón, C. Blanco, F. J. Ferrero, J. C. Viera, N. Bordel, A. Martín, and G. Zissis, "An acoustic resonance band detection workbench for HID lamps," *IEEE Trans. Ind. Appl.*, vol. 43, no. 5, pp. 1191–1198, Sep./Oct. 2007.

[11] F. J. Diaz, F. J. Azcondo, R. Casanueva, Ch. Branas, and R. Zane, "Digital control of a low-frequency square-wave electronic ballast with resonant ignition," *IEEE Trans. Ind. Electron.*, vol. 55, no. 9, pp. 3180–3191, Sep. 2008.

[12] C. S. Moo, C. Y. Yang, C. K. Huang, and C. R. Lee, "Acoustic- resonance-free high-frequency electronic ballast for metal halide lamps," *IEEE Trans. Ind. Elect.*, vol. 55, no. 10, pp. 3653–3660, Oct. 2008.

[13] D. H. J. van Casteren, M. A. M. Hendrix, and J. L. Duarte, "Controlled HID lamp–ballast interaction for low-frequency square-wave drivers," *IEEE Trans. Power Electron.*, vol. 22, no. 3, pp. 780–788, May 2007.

[14] J. M. Alonso, M. A. Dalla Costa, J. Cardesín, J. M. Ramos, and J. García-García, "Small-signal modeling of discharge lamps through step response and its application to low-frequency square-waveform electronic ballasts," *IEEE Trans. Power Electron.*, vol. 22, no. 3, pp. 744–752, May 2007.

[15] J. Melis and O. Vila-Masot, "Low frequency square wave electronic ballast for gas discharge lamps," U.S. Patent 5 428 268, Jun. 27, 1995.

[16] R. Orletti, M. A. Co, D. S. L. Simonetti, and J. L. F. Vieira, "HID lamp electronic ballast with reduced component number," *IEEE Trans. Ind. Electron.*, vol. 56, no. 3, pp. 718–725, Mar. 2009.

[17] Y. T. Huang, H. C. Hsiao, Y. H. Liu, C. R. Lee, and L. L. Lee, "A novel constant-power control for metal-halide lamp electronic ballasts with dimming capability," *IEEE Trans. Plasma Sci.*, vol. 38, no. 6, pp. 1482–1488, Jun. 2010.

[18] C. R. Lee, K. H. Chen, and C. S. Moo, "Operating characteristics of small-wattage metal halide lamps with square wave current from 50Hz to 50kHz," in *Annu. Meet. Conf. Rec. IEEE Ind. Appl. Conf.*, 2003, vol. 2, pp. 1030–1035.

[19] M. Shen, Z. Qian, and F. Z. Peng, "Design of a two-stage low-frequency square-wave electronic ballast for HID lamps," *IEEE Trans. Ind. Appl.*, vol. 39, no. 2, pp. 424–430, Mar./Apr. 2003.

[20] H. Li, M. Shen, Y. Jiang, and Z. Qian, "A novel low-frequency electronic ballast for HID lamps," *IEEE Trans. Ind. Appl.*, vol. 41, no. 5, pp. 1401–1408, Sep./Oct. 2005.

[21] T. J. Liang, C. M. Huang, and J. F. Chen, "Two-stage high-power-factor electronic ballast for metal-halide lamps," *IEEE Trans. Power Electron.*, vol. 24, no. 12, pp. 2959–2966, Dec. 2009.

[22] C. S. Moo, C. K. Huang, K. H. Lee, and D. J. Huang, "Repeatedly resonating ignition circuit for HID lamp electronic ballasts," *IEEE Trans. Ind. Electron.*, vol. 58, no. 1, pp. 244–249, Jan. 2011.

[23] H. J. Chiu, T. H. Song, S. J. Cheng, C. H. Li, and Y. K. Lo, "Design and implementation of a single-stage high-frequency HID lamp electronic ballast," *IEEE Trans. Ind. Electron.*, vol. 55, no. 2, pp. 674–683, Feb. 2008.

[24] C. S. Moo, C. R. Lee, and H. C. Yen, "A high-power-factor constant-frequency electronic ballast for metal halide lamps," in *Proc. IEEE Power Electron. Spec. Conf.*, 1998, vol. 2, pp. 1755–1760.
[25] F. J. F. Martín, C. B. Viejo, J. C. Á. Antón, M. A. P. García, M. Rico-Secades, and J. M. Alonso, "Analysis and design of a high power factor, single-stage electronic ballast for high-intensity discharge lamps," *IEEE Trans. Power Electron.*, vol. 18, no. 2, pp. 558–568, Mar. 2003.
[26] M. A. Dalla Costa, J. M. Alonso, J. Cardesin, J. García, and D. G. Lamar, "A Single-stage high-power-factor electronic ballast based on integrated buck flyback converter to supply metal halide lamps," *IEEE Trans. Ind. Electron.*, vol. 55, no. 3, pp. 1112–1122, Mar. 2008.
[27] I. Batarseh, *Power Electronic Circuits*, NJ: Wiley, 2004.

**Hung-Liang Cheng** (M'08) was born in Chunghwa, Taiwan, in 1964. He received the B.S., M.S., and Ph.D. degrees in electrical engineering all from the National Sun Yat-Sen University, Kaohsiung, Taiwan, in 1986, 1988, and 2001, respectively.

From 1988 to 2007, he was an Electronic Researcher with the Chung-Shan Institute of Science and Technology, Taoyuan County, Taiwan, where he designed and developed high-power transmitters in radar and missile systems. Since February 2007, he has been with the Department of Electrical Engineering, I-Shou University, Kaohsiung, Taiwan, where he is currently an Associate Professor. His current research interests include power-electronic converters and electronic ballasts/drivers for lighting applications.

**Chin-Sien Moo** (M'98) was born in Pingdong, Taiwan, in 1953. He received the B.S., M.S., and Ph.D. degrees in electrical engineering all from the National Chen-Kung University, Tainan, Taiwan, in 1976, 1984, and 1990, respectively.

He was an Electrical Engineer with the Southeast Cement Company from 1976 to 1984. Since 1986, he has been with National Sun Yat-Sen University, Kaohsiung, Taiwan, where he is currently a Professor in the Department of Electrical Engineering. His research interests include power electronic converters and their applications, particularly in lighting electronics and battery systems.

**Chung-Sheng Yang** was born in Kaohsiung, Taiwan, in 1985. He received the B.S. degree in electrical engineering from the National Taipei University of Technology, Taipei, Taiwan, in 2007, and the M.S. degree in electrical engineering from the National Sun Yat-Sen University, Kaohsiung, Taiwan in 2009.

Since October 2009, he has been with the Department of Telecom Power Module R&D, Acbel Polytech Inc., Tamsui, Taipei, Taiwan, where he is currently a Research Engineer. His research interests include power electronic converters and their applications on lighting.

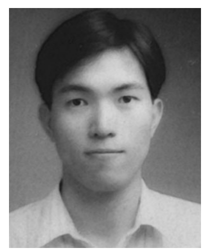

**Chun-Kai Huang** was born in Kaohsiung, Taiwan, in 1972. He received the M.S. and Ph.D. degrees in electrical engineering from the National Sun Yat-Sen University, Kaohsiung, Taiwan, in 2003 and 2011, respectively.

From 1997 to 1999, he was an Electrical Engineer in the Department of High Density Power, Delta Electronics Inc, Chungli, Taiwan, where he was involved in the designing and development of dc/dc power converters for military applications. From 2003 to 2006, he was with the Department of Electronics Engineering, Interpoint Co., Kaohsiung, Taiwan, as a Senior Engineer. Since 2011, he has been a Manager of R&D Center at Longsun Technologies Co., Ltd, Tainan, Taiwan. His research interests include power electronic converters and their applications.